Author Manuscript

Author Manuscript

Author Manuscript

Author Manuscript

HHS Public Access

Author manuscript

J Am Chem Soc. Author manuscript; available in PMC 2019 September 19.

Published in final edited form as:

J Am Chem Soc. 2018 September 19; 140(37): 11777–11783. doi:10.1021/jacs.8b07277.

O_2 Activation by Nonheme Fe^{II} α-Ketoglutarate Dependent Enzyme Variants: Elucidating the Role of the Facial Triad Carboxylate in FIH.

Shyam R. Iyer[†], **Vanessa D. Chaplin**[‡], **Michael J. Knapp**[*,‡], and **Edward I. Solomon**[*,†]

[†]Department of Chemistry, Stanford University, Stanford, California 94305, United States

[‡]Department of Chemistry, University of Massachusetts at Amherst, Amherst, Massachusetts 01003, United States

Abstract

FIH (**F**actor **I**nhibiting **H**IF [Hypoxia Inducible Factor]) is an α-ketoglutarate (αKG)-dependent non-heme iron enzyme that catalyzes the hydroxylation of the C-terminal transactivation domain (CAD) asparagine residue in HIF-1α to regulate cellular oxygen levels. The role of the facial triad carboxylate ligand in O_2 activation and catalysis was evaluated by replacing the Asp201 residue with Gly (D201G), Ala (D201A) and Glu (D201E). Magnetic circular dichroism (MCD) spectroscopy showed that the (Fe^{II})FIH variants were all 6-coordinate (6C) and the αKG plus CAD bound FIH variants were all 5-coordinate (5C), mirroring the behavior of the wild-type (*wt*) enzyme. When only αKG is bound, all FIH variants exhibited weaker Fe^{II}-OH_2 bonds for the sixth ligand compared to wt, and αKG bound D201E was found to be 5C, demonstrating that the Asp201 residue plays an important role in the *wt* enzyme in ensuring that the (Fe^{II}/αKG)FIH site remains 6C. Variable temperature, variable field (VTVH) MCD spectroscopy showed that all the αKG and CAD bound FIH variants, though 5C, have different ground state geometric and electronic structures, which impact their oxygen activation rates. Comparison of O_2 consumption to substrate hydroxylation kinetics revealed uncoupling between the two half reactions in the variants. Thus, the Asp201 residue also ensures fidelity between CAD substrate binding and oxygen activation, enabling tightly coupled turnover.

Abstract

Authors are required to submit a graphic entry for the Table of Contents (TOC) that, in conjunction with the manuscript title, should give the reader a representative idea of one of the following: A key structure, reaction, equation, concept, or theorem, etc., that is discussed in the manuscript. Consult the journal's Instructions for Authors for TOC graphic specifications.

[*]**Corresponding Author:** solomone@stanford.edu mknapp@umass.edu.

Supporting Information

Kinetic endpoint assays, hydrogen peroxide production assays & spectroscopic data not shown in the main text are plotted in the SI. The Supporting Information is available free of charge on the ACS Publications website.

The authors declare no competing financial interest.

Author Manuscript
Author Manuscript
Author Manuscript
Author Manuscript

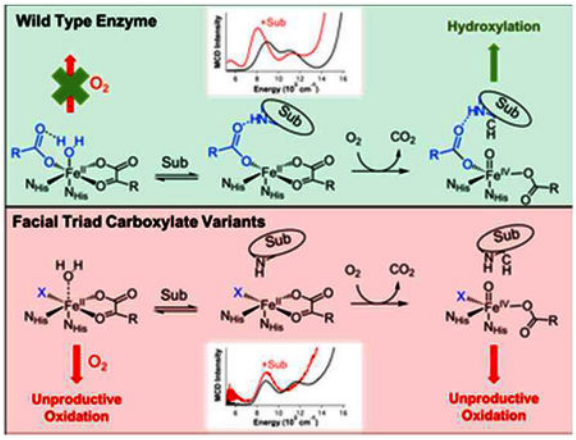

INTRODUCTION

Mononuclear non-heme iron enzymes play important roles in many biological processes including antibiotic, natural product and neurotransmitter biosynthesis, DNA and O_2 regulation and bioremediation.[1–6] These enzymes are divided into different subclasses depending on the cofactor they use, the reactive iron-oxygen intermediates that they proceed through and the type of reaction that they catalyze.[7] These O_2 activating Fe^{II} enzymes generally share a common 2-His-1-carboxylate facial triad motif to bind the Fe center but 3-His and 2-His-1-halide triads also exist.[8] The α-ketoglutarate dependent hydroxylases utilize an Fe^{II} center and α-ketoglutarate (αKG) cofactor to facilitate the 4 electron reduction of dioxygen to perform hydroxylation, halogenation, de-saturation, ring closure or ring expansion on various different substrates.[9] FIH (**F**actor **I**nhibiting **H**IF [Hypoxia Inducible Factor]) is an αKG-dependent asparaginyl hydroxylase that regulates global responses to O_2 levels in mammalian cells by hydroxylating the β-carbon on the Asn-803 residue of the HIF-1α protein (key in shutting off downstream cellular responses).[10,11] Under conditions of low O_2 (i.e. hypoxia), the non-hydroxylated HIF-1α dimerizes with the HIF-1β protein, binds transcriptional machinery and activates genes leading to angiogenesis and erythropoiesis, which results in an increase in vascularization and cellular O_2 levels.[5,12] Studying the tightly regulated function of this enzyme provides insight into the factors that govern its highly selective reactivity and the design of better therapeutic strategies.[13,14]

αKG-dependent enzymes follow a general mechanistic strategy where the active site remains 6-coordinate (6C) until both cofactor and substrate are bound, resulting in a coordinatively unsaturated 5-coordinate (5C) site capable of reacting with dioxygen.[7,9,15] These 5C sites activate O_2 to form reactive Fe^{IV}=O moieties that then attack the associated substrate to form product and regenerate the Fe^{II} site (Scheme 1). αKG-dependent enzymes can also carry out uncoupled O_2 reactivity, where the αKG is oxidized but product is not formed.[16,17] This would be highly unfavorable in an enzyme like FIH as this would dysregulate gene expression from cellular O_2 levels, leading to oxidative damage and apoptosis.[5] Our previous study of *wt*-FIH computationally showed that the facial triad carboxylate plays a key role in ensuring that the FIH active site remains 6C when only αKG is bound by hydrogen bonding with a H_2O ligand (see scheme 1, *top middle*),[18–20] which is

Author Manuscript Author Manuscript Author Manuscript Author Manuscript

weakly bound due to the strong donor interaction of the αKG with the Fe^{II}. This is important because this αKG bound site has all 4 electrons needed for O_2 activation and loss of the water ligand can lead to premature Fe^{IV}=O formation, which would result in autooxidation or enzyme inactivation.[16,17]

The FIH D201X (D201G/D201A/D201E) enzymes are the first reported facial triad variants in an αKG-dependent enzyme that are capable of binding Fe^{II}.[21] Furthermore, D201G is able to hydroxylate the C-terminal transactivation domain (CAD) of a truncated form of the HIF-1α substrate at up to half the efficiency of the native enzyme in the presence of added chloride (referred to as D201GCl).[20] However, the other variants are comparatively unreactive in substrate hydroxylation. This loss in activity can be due to the inability to form the 5C site required for O_2 activation or the inability of the resultant Fe^{IV}=O moiety to properly react with the substrate. Previous studies of these enzyme variants focused on substrate hydroxylation and not coordination changes at the Fe^{II} center.[20] However, these variants reveal perturbations that provide mechanistic insight into the role of the carboxylate in controlling the Fe^{II} site, thus the timing of O_2 activation. In this study, we have used magnetic circular dichroism (MCD) spectroscopy to define the coordination number and geometry of the different D201X-Fe^{II} variants and their interaction with αKG and CAD cosubstrates and correlated these structural changes with O_2 consumption kinetics to characterize the role of the facial triad carboxylate in O_2 activation for enzyme function.

MATERIALS AND METHODS

Materials and Enzyme Purification.

All reagents were purchased from commercial vendors and used as received, with the exception of CAD substrate. CAD was purchased (EZBiolab, Carmel, IN, USA) as a desalted peptide and further purified by reverse phase HPLC methods. Point mutations to Asp201 were made using the QuickChange mutagenesis kit (Stratagene) in the pET28a-FIH construct. The resulting plasmid DNA was sequenced (Genewiz, NJ, USA) to confirm the point mutation. His_6-WT FIH and the His_6-D201X variants were overexpressed in BL21-DE3 *E. coli* and purified as previously described.[18] Briefly, the cell pellet was lysed using sonication, centrifuged, then dialyzed into 10 mM Tris pH 8.00 to remove EDTA from the lysis buffer. Centrifugation of the supernatant further clarified the lysate prior to loading on to a Ni-NTA column. After loading the lysate, the column was washed with 5 column volumes each of 100% A buffer (50 mM Tris pH 8.0, 300 mM NaCl, 15 mM Imidazole) and 15% B buffer (50 mM Tris pH 8.0, 300 mM NaCl, 250 mM Imidazole) before eluting the His_6-FIH protein with 100% B buffer. Thrombin was then added to the eluent to cleave the His_6 tag for 36 hours at 4 °C. The cleaved FIH was loaded on to the Ni-NTA again to remove the His_6 tag and any remaining uncleaved protein. Overnight incubation with 50 mM EDTA removed exogenous metals. Size exclusion chromatography was then used to separate the protein from the thrombin and EDTA. Purified protein was aliquotted and stored at 20 °C in 50 mM HEPES pH 7.00. Protein purity (>95%) was evaluated using SDS-PAGE.

Author Manuscript Author Manuscript Author Manuscript Author Manuscript

MCD Spectroscopy.

Apo-D201X(FIH) variants were buffer exchanged into deuterated 50mM HEPES buffer (pD 7.5) at 4°C. For the D201GCl samples, 100mM NaCl was added to the buffering system. Protein was degassed in an ice bath, transferred into a nitrogen atmosphere maintained in a Vacuum Atmosphere Nexus-1 glovebox (<2 ppm oxygen) and stirred at 4°C. 1 eq of ferrous ammonium sulfate, 10 eq αKG and 2.5 eq CAD were added and equilibrated for 15 mins each. Samples were then saturated with deuterated sucrose and loaded into an MCD cell. Near-IR (600nm – 200nm) MCD spectroscopy was performed using a JASCO J-730 spectropo larimeter equipped with an InSb photodiode detector cooled with liquid nitrogen and fitted with an Oxford Instruments SM4000–7T superconducting magnet. UV-Vis MCD (300nm – 900nm) spectroscopy was performed using a JASCO J-810 spectropolarimeter equipped with a photomultiplier tube and fitted with an Oxford Instruments SM4000–7T superconducting magnet. The sample temperature was measured using a calibrated Cernox resistor from Lakeshore Cryotronics. MCD spectra were corrected for zero-field baseline effects by subtracting the corresponding 0T scan from the data. Variable temperature, variable field (VTVH) MCD isotherms were collected at 6–8 temperatures between 2 and 25K and at 12 fields between 0 and 7T.

Kinetic Methods – O_2 Consumption and CAD hydroxylation assays.

An Oxygraph Plus System (Hansatech) was used to monitor the amount of oxygen consumed by the enzyme. This oxygen sensor contains a central reaction vessel surrounded by a water jacket, with a Clark-type electrode disc at the bottom of the reaction vessel. The electrode disc utilized a KCl bridge and a PTFE membrane that is selectively permeable to oxygen molecules. A new membrane was prepared and calibrated each day with air saturated water and dithionite. 400 μL reactions were equilibrated at atmospheric O_2 in the reaction vessel at 37 °C until a stable baseline was achieved. Assays were initiated with cold purified FIH (10 μM) using a Hamilton gas-tight syringe. The rate of O_2 consumption was monitored over time until the rate of O_2 consumption resembled the baseline slope. Assays contained 100 μM αKG, 50 μM $FeSO_4$, 80 μM CTAD and 10 μM FIH in 50 mM HEPES pH 7.00, and 50 μM ascorbate. Controls were performed to determine the optimal amount of ascorbate that could be used to minimize baseline slope while retaining maximal FIH activity. 5 μL of each reaction was then quenched in 20 μL of matrix (3,5-dimethoxy-4-hydroxycinnamic acid saturated in 75% ACN/0.2% TFA) and analyzed by MALDI-TOF-MS (Ultra-flex, Bruker) monitoring the +1 charge state of the substrate (CAD) and the product (hydroxylated CAD).

RESULTS AND ANALYSIS

MCD Spectroscopy.

Low temperature (LT) MCD spectroscopy in the near-infrared (NIR) region is a powerful tool for studying Fe^{II} active sites as it probes $^5T_2 \rightarrow {}^5E$ ligand field (LF) transitions, which reflect coordination geometry. LF transitions, though weak in absorption spectroscopy, are intense in MCD at low temperatures due to different selection rules.[22] We have calibrated this methodology by assigning the transition energies and excited state splittings (Δ^5E, see Fig. 1A *top*) of a variety of 6C, 5C and 4C model complexes with different geometries.[22–24]

Author Manuscript Author Manuscript Author Manuscript Author Manuscript

Briefly, two transitions centered around 10,000 cm^{-1} split by ~2,000 cm^{-1} is indicative of a distorted 6C site. Removal of an axial ligand leads to a 5C square pyramidal (SP) structure with one transition above 10,000 cm^{-1} and one around ~5,000 cm^{-1}. Alternatively, a 5C trigonal bipyramidal (TBP) site exhibits one transition around or less than 10,000 cm^{-1} and one <5,000 cm^{-1} (often undetectable). Finally, 4C distorted tetrahedral sites exhibit two transitions around ~6,000–7,000 cm^{-1}.

The LT MCD spectra of the resting Fe^{II}-bound sites (Fig. 1A) of all these variants including D201GCl show two transitions centered around 10,000 cm^{-1} with Δ^5E ~ 1,800 cm^{-1}, thus all are 6C distorted octahedral sites. There are some small differences in the excited state splittings (Table 1) reflecting small changes in the ligand field due to the variation of the D201 replacement ligand. In the absence of the carboxylate ligand, D201A and D201G likely have a water-derived ligand, i.e. H_2O or OH[6], bound to the Fe^{II} center. The excited state splitting of D201GCl relative to D201G is greater by 150 cm^{-1} and intensity ratios of the two transitions are slightly perturbed (Fig. S1). This evidence, combined with X-ray absorption spectroscopy performed on the (Fe^{II}/N-oxalylglycine)D201GCl site,[25] argues for a Cl^- ion binding to the Fe^{II} center in the D201GCl resting site. Finally, these resting Fe^{II} spectra are also similar to that of the *wt* enzyme, thus all have Fe^{II} bound with 2 His and 3 H_2O ligands with the 6th ligand position being a monodentate carboxylate or a Cl[6] or another water-derived ligand.

In the Fe^{II}/αKG site for *wt*-FIH (Fig. 1B, *top*), there are two transitions centered around 10,000 cm^{-1} with Δ^5E of 2,300 cm^{-1}.[19] This splitting is larger than that observed for many other 6C sites in the literature and is attributed to the weakening of the Fe^{II}-OH_2 bond of the 6th ligand due to the strong donor interaction associated with the αKG-bound to the Fe^{II}.[26,27] The Fe^{II}/αKG sites of D201A and D201G are both similar to *wt*-FIH and also have two transitions centered around 10,000 cm^{-1} with Δ^5E splittings of 2,300 and 2,400 cm^{-1} respectively (Fig. 1B, *purple* and *blue* respectively & Table 1), indicating that they are 6C but with a weak water ligand. (Fe^{II}/αKG)D201E has two transitions centered at 10,000 cm^{-1} with Δ^5E of ~2,700 cm^{-1} (Fig. 1B, *green*, Table 1). This observed splitting is large compared to the other 6C sites observed in αKG-dependent enzymes[19,26] and likely indicates a site with a very weakly bound/unbound 6th ligand. (Fe^{II}/αKG)D201GCl has two transitions centered around 10,000 cm^{-1} and a third transition at ~7,400 cm^{-1} (Fig. 1B, *red*, Table 1*)*, indicating a mixture of two different Fe^{II} sites (note that a single Fe^{II} site can only have two LF transitions in this energy region). The ground state associated with the low energy transition has been investigated using VTVH MCD to determine if it arises from a 5C or 6C site (*vide infra*). All the (Fe^{II}/αKG)D201X spectra show a transition tailing into the NIR spectral region from higher energy that is due to the Fe^{II}-to-αKG metal-to-ligand charge transfer transitions observed around 20,000 cm^{-1} (Figure S2), which are also present in αKG bound *wt*-FIH and other αKG-dependent enzymes. [19,26,27] This demonstrates that the αKG is bound to the Fe^{II} site in a similar bidentate manner to the *wt* enzyme in the variants and has replaced two water ligands from the resting sites.

The ternary (Fe^{II}/αKG/CAD)D201X spectra all have more than 2 LF transitions, thus are all mixtures of two different Fe^{II} sites and all show substantial differences in the energy positions and excited state splittings of their LF transitions (Fig. 1C & Table 1).

Author Manuscript Author Manuscript Author Manuscript Author Manuscript

Additionally, they all have Fe^{II}-to-αKG charge transfer transitions at similar energies (~20,000 cm^{-1}), demonstrating that αKG is analogously bound in a bidentate manner in these active sites (Fig. S2). *wt*-FIH has 4 transitions at <5,000, 7,950, 9,000 and 11,150 cm^{-1}; the presence of one band around 5,000 cm^{-1} indicates that it is a 5C/6C mixture.[19] For the glycine variants, D201GCl (Fig. 1C, *red*) has four observed transitions at <5,000, 6,200, 9,250 and 10,900 cm^{-1} whereas D201G (Fig. 1C, *blue*) has four transitions at <5,000, 6,100, 8,800 and 11,350 cm^{-1}. These sites have different energy LF transitions and geometries due to the presence of the Cl^- ligand in D201GCl. Importantly, both sites have two transitions at <5,000 and ~ 6,000 cm^{-1}, which demonstrate that they are both 5C/5C mixtures with one square pyramidal component (from the >10,000 cm^{-1} feature). The D201E site (Fig. 1C, *green*) has three observed transitions at ~9,000, 11,500 and 14,000 cm^{-1}. The high energy of the 14,000 cm^{-1} LF transition requires one of the sites to be square pyramidal. Finally, D201A (Fig. 1C, *purple*) shows a low energy transition at <5,000 cm^{-1}, along with two bands around 10,000 cm^{-1} demonstrating that it has at least one 5C component as well. Together, these data demonstrate that when both cofactor and substrate are bound all the variants have coordinatively unsaturated 5C Fe^{II} sites with an open position for the O_2 reaction.

VTVH MCD Spectroscopy.

Variable temperature, variable field (VTVH) MCD spectroscopy uses an excited state transition to probe the ground state. This involves measuring the temperature and field dependence of the MCD intensity of a particular transition. For Fe^{II} systems, fitting these data using a non-Kramers doublet model[22,23] provides detailed information on the S=2 ground state zero-field splitting (ZFS), which in turn gives the sign and magnitude of the tetragonal splitting (Δ) between the $d_{xz,yz}$ and d_{xy} orbitals and the rhombic splitting (V) between d_{xz} and d_{yz} of the Fe^{II} ground state. These parameters, coupled with the LF excited state data obtained from the LT MCD spectra, give a complete picture of the ligand field around the iron center and allow for the detailed description of the electronic and geometric structure of the Fe^{II} active site. The analysis presented below focuses on trends in the values of Δ, which correlate with coordination number and π interactions with the ligands. Note that a positive value of Δ is reflected in the saturation magnetization data through a large nesting (i.e. spread) of the isotherms (Fig. 2, *top right*), while a negative value of Δ is reflected in a small nesting (Fig. 2, *top left*).[22]

MCD spectroscopy on the resting Fe^{II}-bound sites showed that they are all similar and VTVH MCD data previously collected for the *wt* enzyme at 8,200 cm^{-1} (Figure S3A) were fit with Δ = −275 cm^{-1}, which is typical for 6C distorted octahedral sites.[22] The arrows in Fig. 1 show the energies at which the VTVH MCD data were collected and Table 2 (*middle*) summarizes the ground state parameters obtained for the αKG bound Fe^{II} complexes. Data collected at 8,200 cm^{-1} for the αKG bound *wt* enzyme (Fig. S3B), a 6C site from the excited state splitting (Δ^5E), show an increase in magnitude of Δ to −950 cm^{-1} relative to the resting site. This increase in magnitude is due to the back-bonding of the Fe^{II} into the π* orbital of the αKG and is well documented in the αKG-dependent hydroxylases.[19,26] From the MCD spectroscopy on the (Fe^{II}/αKG)D201GCl site, there were three transitions present, with one at low energy (Fig. 1B). To address the coordination number of the low energy

Author Manuscript Author Manuscript Author Manuscript Author Manuscript

component of this mixture of Fe^{II} sites, VTVH MCD data were collected at 7,100 cm^{-1} (Fig. 2, *top left*) and fit with $\Delta = -950$ cm^{-1}, similar to the *wt* enzyme, suggesting that this band arises from a 6C site. Thus, the second transition associated with this low energy feature should be at higher energy and overlapped by the additional components present. The lower energy for these transitions associated with the second site could be due to the presence of the chloride ligand. VTVH MCD data were not measured for the other bands in D201GCl due to spectral overlap. Data for (Fe^{II}/αKG)D201E collected at 8,560 cm^{-1} (Figure S4) were fit with $\Delta = -1{,}100$ cm^{-1}. This larger $|\Delta|$ is similar to the values observed for the 5C ternary complexes (*vide infra*) and, combined with the relatively large value for Δ^5E (2,700 cm^{-1}), suggests that this site is either 6C with a very weak axial ligand or 5C square pyramidal with unbound axial ligand (i.e. loss of H_2O). Data collected for αKG bound D201G at 11,100 cm^{-1} and D201A at 11,430 cm^{-1} (Fig. 2, *top right* and Fig. S5) were fit with positive values of U (due to their large nesting behavior) of 950 and 700 cm^{-1} respectively, consistent with the 6C geometry observed from their excited state splittings (Table 1). The VTVH MCD data on the αKG only bound Fe^{II} sites show that, apart from D201E, the variants are 6C, though with different ground states and larger excited state splittings compared to the *wt* enzyme.

The bottom panel in Figure 2 (along with Fig. S3C and S6) present the saturation magnetization behavior observed among the ternary (cofactor and substrate bound) complexes of *wt*-FIH, D201GCl, D201G and D201A and the ground state parameters for these ternary complexes are summarized in Table 2 (*bottom*). Due to overlapping bands and sample concentration issues, useful VTVH MCD data on the ternary complex of D201E could not be obtained. Data on the *wt* enzyme collected at 7,550 cm^{-1} (Figure S2C) were fit with $\Delta = -1{,}200$ cm^{-1}. This increase in the magnitude of U relative to the αKG only bound site (where $\Delta = -950$ cm^{-1}) is consistent with a 5C structure. [19] Unlike the *wt* enzyme, the ternary complexes of the variants were all fit with positive values of Δ due to their large nesting behaviors. Since all these variants are 5C, this change in sign of Δ correlates with the replacement of the carboxylate equatorial ligand (in the *wt* enzyme) with the chloride or water-derived ligand and has implications with respect to the observed O_2 reactivity (*vide infra*). Data on D201GCl collected at 6,430 cm^{-1} (Figure 2, *bottom left*) were fit with $\Delta =$ 1,150 cm^{-1}, similar in magnitude to the *wt*-FIH ternary site, and the difference between the binary and ternary complex Δ values is also consistent with a 6C → 5C conversion. Data collected for the ternary complexes of D201G at 5,500 cm^{-1} (Figure 2, *bottom right*) and D201A at 5,200 cm^{-1} (Fig. S6) were fit with Δ values of 1,000 cm^{-1} and 700 cm^{-1} respectively. Though the differences in Δ between the αKG bound and the ternary complex (Table 2) for these variants are small, the presence of low energy transitions in the MCD spectra (in Fig. 1C) show that they are 5C. VTVH MCD on the ternary complexes of the variants show that, though they are all 5C, they have different coordination environments and geometries, and this is reflected in their observed O_2 reactivities (*vide infra*).

O_2 Consumption and Substrate Hydroxylation Kinetics.

From the LT MCD and VTVH MCD spectroscopy presented above, 5C sites are present in all the ternary complexes and possibly in the (Fe^{II}/αKG)D201E complex. The presence of a 5C site with αKG bound should enable O_2 activation and this was tested using a Clark O_2

Author Manuscript Author Manuscript Author Manuscript Author Manuscript

sensor to track O_2 consumption. Table 3 summarizes the O_2 consumption rates of all the ternary and the (Fe^{II}/αKG)D201E complex. The other αKG only bound *wt* and variant enzymes that are 6C from MCD did not show measurable O_2 consumption, confirming that a 5C site correlates with O_2 activation. Compared to the *wt*-FIH ternary complex, all the variants react with O_2 at >10-fold slower rates. Furthermore, there are differences in the O_2 consumption rates among the variants. The (Fe^{II}/αKG)D201E, (Fe^{II}/αKG/CAD)D201E and (Fe^{II}/αKG/CAD)D201GCl sites react with O_2 at similar rates of 1.7 min^{-1}, 1.7 min^{-1} and 1.9 min^{-1} respectively. The D201G ternary complex, which is also a 5C/5C mixture like (Fe^{II}/αKG/CAD)D201GCl, consumes O_2 at a rate of 0.3 min^{-1}, while the D201A ternary complex does not show consumption of O_2 above the background (ascorbate reacting with O_2), i.e. < 0.01 min^{-1}. Thus, the differences in 5C geometries from MCD (Table 1 & 2) lead to greater than 2 orders of magnitude variation in the O_2 consumption rates.

Comparing the rates of substrate hydroxylation to O_2 consumption in Table 3 shows that, in contrast to *wt* where both rates are the same within error, substrate hydroxylation is slower than O_2 consumption for all the variants. This demonstrates that the two half reactions, i.e. O_2 activation and substrate hydroxylation, are uncoupled, which is confirmed through the end point analysis assays presented in Table S1. It is also important to note that these reactions only produce marginal amounts of H_2O_2 as a byproduct (Table S1). This, coupled with the observation that succinate is produced[20], suggest that most of the O_2 equivalents used by these variants produce an Fe^{IV}=O intermediate capable of reacting with substrate. Furthermore, since the rates of substrate hydroxylation are an order of magnitude lower than the O_2 consumption, the second half of the reaction involving substrate hydroxylation is far more impaired by the D201X variants.[17,18,28] Together, these data show that the 5C sites do consume O_2 (albeit at different and lower rates than *wt*) and that the variants show a decrease in their coupling ratios demonstrating that there is also a loss in substrate hydroxylating efficiency due to the mutation of the D201 facial triad ligand.

DISCUSSION

This study presents new insights into the geometric and electronic structures and O_2 consumption reactivity of the Fe^{II} active sites in the facial triad carboxylate variants of FIH. MCD spectroscopy on the resting sites shows that all the variants bind Fe^{II} and are all 6C with similar Δ^5E splittings of ~1,800 cm^{-1}. All the variants thus have 2 histidines, 3 waters with a 6th Cl^6 (D201GCl), carboxylate (D201E) or water-derived (D201A, D201G) ligand bound to the Fe^{II} center.

The structures of all the variants substantially change when αKG is bound to the active site. From the MCD data, the Fe^{II}-to-αKG metal to ligand charge transfer transitions are observed at similar energies as *wt*, suggesting that αKG is analogously bound bidentate with the replacement of two water ligands in all the (Fe^{II}/αKG)D201X sites. All the variants, except D201E, are 6C but with larger Δ^5E splittings (Table 1) than the wild-type enzyme. This supports the predicted role of the facial triad carboxylate in stabilizing the binding of the sixth water ligand through a hydrogen bond to its distal oxygen, as mutations eliminating this carboxylate lead to the weakening of this Fe^{II}-OH_2 bond.

Author Manuscript Author Manuscript Author Manuscript Author Manuscript

VTVH MCD on (Fe^{II}/αKG)D201E showed that it has a ground state splitting (Δ) of 1,200 cm^{-1} (Table 2), similar to the ternary 5C active sites, and the largest Δ^5E splitting in αKG only bound sites of 2,700 cm^{-1}. It is also the only αKG bound Fe^{II} variant that reacts with O_2 in the absence of substrate (Table 3). From crystallography performed on this variant, the presence of the extra methyl group on the carboxylate affects its orientation relative to the Fe^{II} center such that it has a steric clash between its unbound O and the position where the sixth water ligand would bind, resulting in the 5C site with a monodentate carboxylate or a 6C site with a very weakly bound distal O of the glutamate residue.[20] From computational studies on *wt*, a similar steric clash between asparagine on the CAD substrate and the water ligand bound to the Fe^{II} center leads to H_2O dissociation and an open coordination position for O_2 reactivity.[29] Coupled with the MCD results on the (Fe^{II}/αKG)D201E site, the steric interaction with the sixth water ligand is an important factor along with the donation of the αKG in determining the 6C → 5C conversion in the FIH active site.

VTVH MCD data on the ternary (Fe^{II}/αKG/CAD)D201X complexes show that their ground state splittings (Δ) are oppositely signed compared to the *wt* enzyme (Table 2). The change in sign of Δ, due to the replacement of the carboxylate ligand with a Cl^- or a water derived ligand, is significant as it demonstrates that the unpaired electron in the d manifold of the highspin Fe^{II} center, that is crucial for O_2 activation, is now in a different redox active molecular orbital. This change is reflected in the O_2 consumption kinetics as all the variants consumed O_2 at rates more than 10-fold slower than the wildtype enzyme. Furthermore, from MCD spectroscopy on these ternary sites, all the variants have 5C components with their LF transitions at different energies, indicating structurally inequivalent active sites. These structural changes are manifested in the O_2 consumption rates as they vary by more than two orders of magnitude across the variants. Though these O_2 consumption rates are significantly different, it is important to note that, in terms of the $\Delta\Delta G^{\ddagger}$ for the O_2 activation reaction, these rate differences only correspond to a change in activation barrier of <3 kcal/mol relative to the *wt* barrier of ~15 kcal/mol. Thus, the carboxylate ligand of the facial triad is crucial in tuning the electronics of the ternary active site, such that the redox active molecular orbital is properly oriented for O_2 activation.

Comparing the O_2 consumption rate to the CAD hydroxylation rate showed that all the variants performed uncoupled turnover. D201 plays an important role in docking the CAD substrate in the native reaction by hydrogen bonding with an amide group in the backbone of the substrate (Fig. 3).[17,28] From these O_2 consumption and substrate hydroxylation kinetics, the variants react with O_2 to form an Fe^{IV} =O but appear to be poorly positioned to react with the substrate through hydrogen atom abstraction (HAA), followed by rebound hydroxylation. Since these variants have structurally distinct 5C sites, changes in the orientation of the CAD substrate with respect to the Fe^{IV}=O would result in dissipation of the high-valent intermediate through enzyme inactivation or reduction (normally by the excess ascorbate in the assays).[16,18]

It is interesting to note that while D201GCl has a chloride bound perpendicular to the open position on the Fe, only hydroxylation is observed. We have previously shown that the HAA reaction performed by non-heme Fe^{IV}=O intermediates can proceed through two possible channels: a σ-channel that is active for HAA along the Fe-O bond and a π-channel that

Author Manuscript Author Manuscript Author Manuscript Author Manuscript

performs HAA perpendicular to the Fe-O bond. While the π-channel can hydroxylate or halogenate depending on the positioning of carbon radical product (formed after HAA) relative to the OH^- or Cl^- equatorial ligand, the σ HAA channel produces a radical oriented along the Fe^{III}-OH bond and can only lead to substrate hydroxylation.[30,31] From the crystal structure in Fig. 3, the CAD substrate docks directly above the open coordination position in the Fe^{II} active site. This is consistent with FIH being oriented to use the Fe=O σ-channel for HAA leading to hydroxylation but not halogenation.

In summary, steric interaction with the sixth water ligand through either the substrate or an active site residue is the factor that determines the 6C to 5C conversion in FIH. The facial triad carboxylate in FIH plays key roles in ensuring that the 5C Fe^{II} center has the proper electronics for facile O_2 activation and that the substrate is bound in the correct orientation for coupled HAA.

Supplementary Material

Refer to Web version on PubMed Central for supplementary material.

ACKNOWLEDGMENT

This research was supported by the U.S. National Institutes of Health grants GM 77413 (M.J.K) and GM 40392 (E.I.S.).

REFERENCES

(1). Baldwin JE; Abraham E Nat. Prod. Rep 1988, 5 (2), 129. [PubMed: 3145474]

(2). Vaillancourt FH; Yin J; Walsh CT Proc. Natl. Acad. Sci 2005, 102 (29), 10111–10116. [PubMed: 16002467]

(3). Fitzpatrick PF Annu. Rev. Biochem 1999, 68 (1), 355–381. [PubMed: 10872454]

(4). Gerken T; Girard CA; Tung Y-CL; Webby CJ; Saudek V; Hewitson KS; Yeo GSH; McDonough MA; Cunliffe S; McNeill LA; Galvanovskis J; Rorsman P; Robins P; Prieur X; Coll AP; Ma M; Jovanovic Z; Farooqi IS; Sedgwick B; Barroso I; Lindahl T; Ponting CP; Ashcroft FM; O'Rahilly S; Schofield CJ Science 2007, 318 (5855), 1469–1472. [PubMed: 17991826]

(5). Wenger RH J. Exp. Biol 2000, 203, 1253–1263. [PubMed: 10729275]

(6). Gibson DT; Parales RE Curr. Opin. Biotechnol 2000, 11 (3), 236–243. [PubMed: 10851146]

(7). Solomon EI; Light KM; Liu LV; Srnec M; Wong SD Acc. Chem. Res 2013, 46, 2725–2739. [PubMed: 24070107]

(8). Que L, Jr. Nature 2000, 7 (3), 182–184.

(9). Solomon EI; Goudarzi S; Sutherlin KD Biochemistry 2016, 55 (46), 6363–6374. [PubMed: 27792301]

(10). Hewitson KS; McNeill LA; Riordan MV; Tian Y-M; Bullock AN; Welford RW; Elkins JM; Oldham NJ; Bhattacharya S; Gleadle JM; Ratcliffe PJ; Pugh CW; Schofield CJ J. Biol. Chem 2002, 277, 26351–26355. [PubMed: 12042299]

(11). Elkins JM; Hewitson KS; McNeill LA; Seibel JF; Schlemminger I; Pugh CW; Ratcliffe PJ; Schofield CJ J. Biol. Chem 2003, 278, 1802–1806. [PubMed: 12446723]

(12). Semenza GL Genes Dev 2000, 14 (16), 1983–1991. [PubMed: 10950862]

(13). Nagel S; Talbot NP; Mecinovic J; Smith TG; Buchan AM; Schofield CJ Antioxid. Redox Signal 2010, 12, 481–501. [PubMed: 19754349]

(14). Hewitson KS; Schofield CJ Drug Discov. Today 2004, 9, 704–711. [PubMed: 15341784]

(15). Zhou J; Kelly WL; Bachmann BO; Gunsior M; Townsend CA; Solomon EI J. Am. Chem. Soc 2001, 123 (30), 7388–7398. [PubMed: 11472170]

Author Manuscript Author Manuscript Author Manuscript Author Manuscript

(16). Liu A; Ho RYN; Que L; Ryle MJ; Phinney BS; Hausinger RP J. Am. Chem. Soc 2001, 123 (21), 5126–5127. [PubMed: 11457355]

(17). Chen Y-H; Comeaux LM; Eyles SJ; Knapp MJ Chem. Commun. (Camb) 2008, 4768–4770. [PubMed: 18830487]

(18). Chen Y-H; Comeaux LM; Herbst RW; Saban E; Kennedy DC; Maroney MJ; Knapp MJ J. Inorg. Biochem 2008, 102, 2120–2129. [PubMed: 18805587]

(19). Light KM; Hangasky JA; Knapp MJ; Solomon EI J. Am. Chem. Soc 2013, 135, 9665–9674. [PubMed: 23742069]

(20). Hangasky JA; Taabazuing CY; Martin CB; Eron SJ; Knapp MJ J. Inorg. Biochem 2017, 166, 26–33. [PubMed: 27815979]

(21). Hewitson KS; Holmes SL; Ehrismann D; Hardy AP; Chowdhury R; Schofield CJ; McDonough MA J. Biol. Chem 2008, 283, 25971–25978. [PubMed: 18611856]

(22). Solomon EI; Pavel EG; Loeb KE; Campochiaro C Coord. Chem. Rev 1995, 144, 369–460.

(23). Solomon EI; Brunold TC; Davis MI; Kemsley JN; Lee S; Lehnert N; Neese F; Skulan AJ; Yang Y; Zhou J Chem. Rev 2000, 100, 235–349. [PubMed: 11749238]

(24). Pavel EG; Kitajima N; Solomon EI J. Am. Chem. Soc 1998, 120 (6), 3949–3962.

(25). This is manuscript is under review at Inorganic Chemistry: ic-2018-01736q “Ligand substitution supports O_2 activation in facial triad variants of FIH, an αKG dependent oxygenase.” Chaplin, Vanessa; Hangasky, John; Huang, Hsin-Ting; Duan, Ran; Maroney, Michael; Knapp, Michael.

(26). Pavel EG; Zhou J; Busby RW; Gunsior M; Townsend C. a.; Solomon EI J. Am. Chem. Soc 1998, 120 (4), 743–753.

(27). Neidig ML; Brown CD; Light KM; Fujimori DG; Nolan EM; Price JC; Barr EW; Bollinger JM; Krebs C; Walsh CT; Solomon EI J. Am. Chem. Soc 2007, 129 (46), 14224–14231. [PubMed: 17967013]

(28.) Saban E; Flagg SC; Knapp MJ J. Inorg. Biochem 2011, 105, 630–636. [PubMed: 21443853]

(29). Light KM; Hangasky JA; Knapp MJ; Solomon EI Dalt. Trans 2014, 43 (4), 1505–1508.

(30). Srnec M; Solomon EI J. Am. Chem. Soc 2017, 139 (6), 2396–2407. [PubMed: 28095695]

(31). Srnec M; Wong SD; England J; Que L, Jr.; Solomon EI Proc. Natl. Acad. Sci. U. S. A 2012, 109, 14326–14331. [PubMed: 22908238]

Author Manuscript Author Manuscript Author Manuscript Author Manuscript

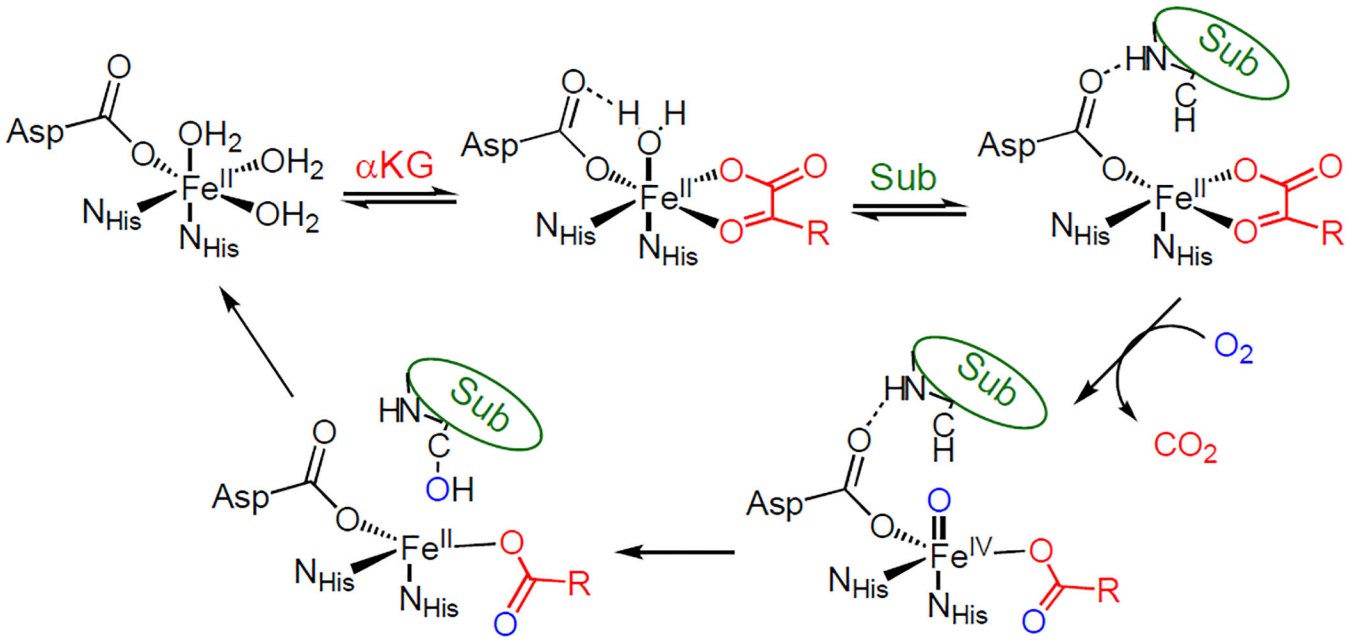

Scheme 1.
Reaction mechanism for the αKG-dependent hydroxylases

Author Manuscript Author Manuscript Author Manuscript Author Manuscript

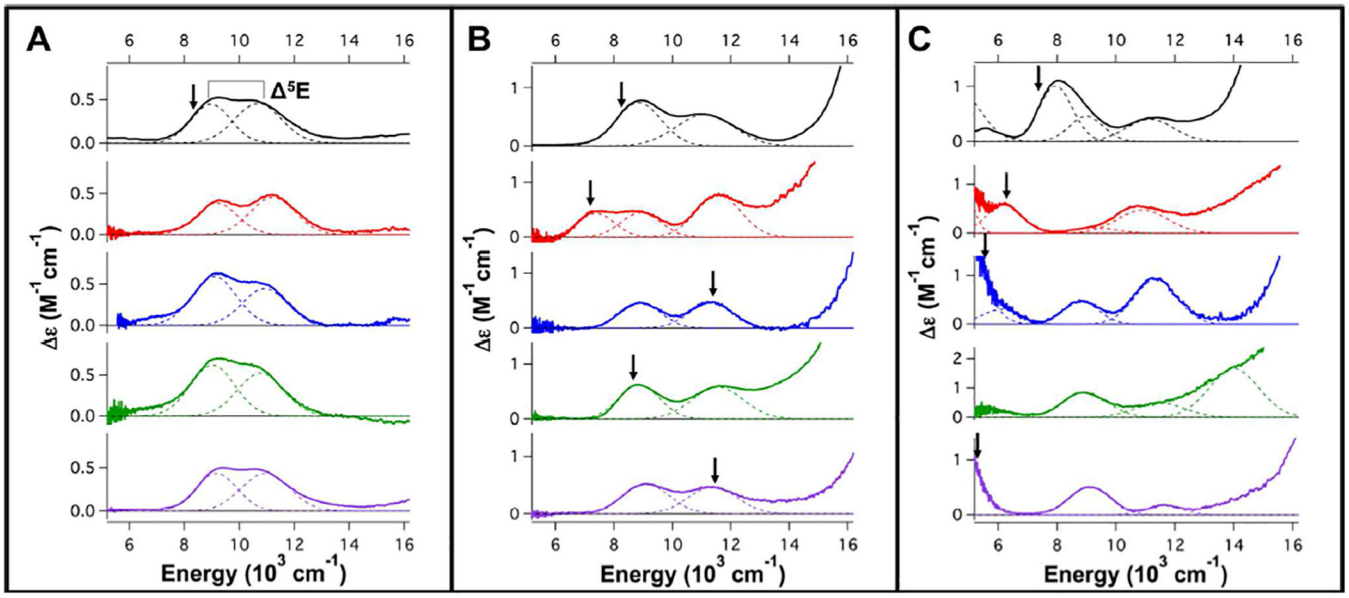

Figure 1.

5K, 7T MCD spectra of *wt*-FIH(black), D201GCl(red), D201G(blue), D201E(green) and D201A(purple). A) Fe^{II}-loaded resting sites, B) Fe^{II}/αKG sites and C) Fe^{II}/αKG/CAD ternary sites. In A, B and C, the Gaussianresolved band energies and Δ^5E splittings are summarized in Table 1. The arrows indicate the energies at which VTVH data were collected for each sample.

Author Manuscript Author Manuscript Author Manuscript Author Manuscript

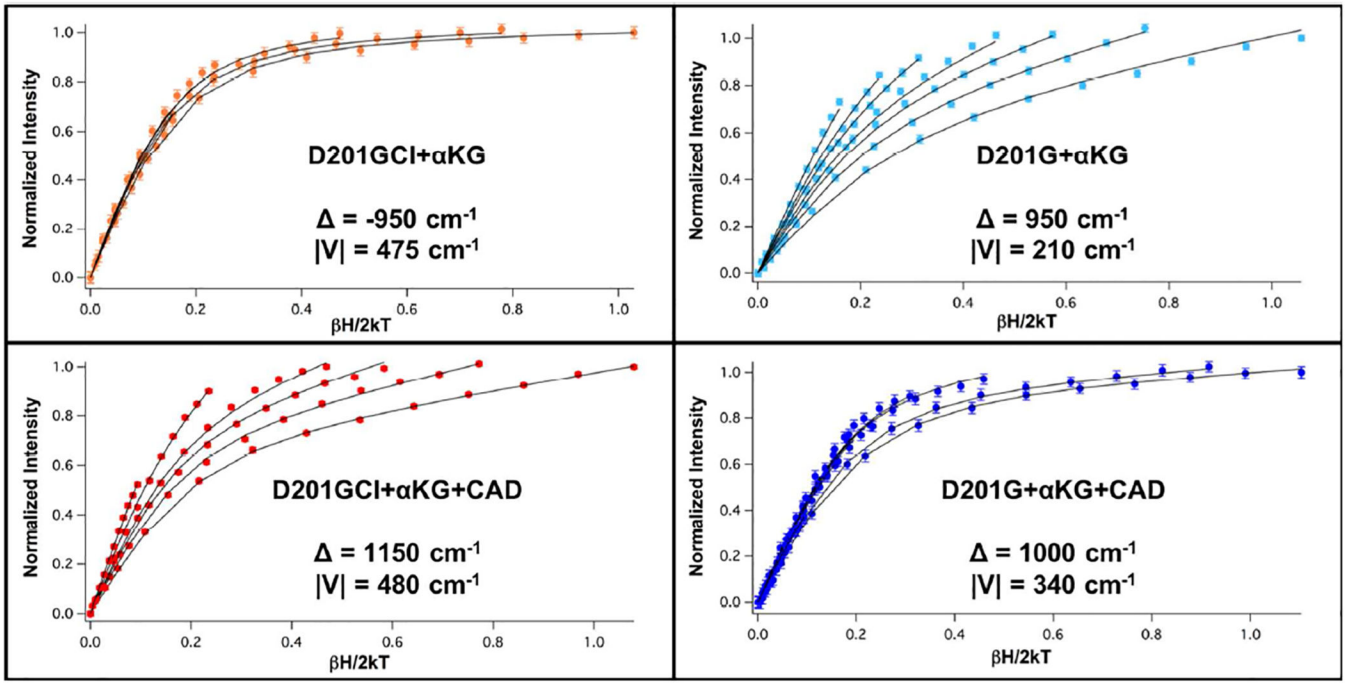

Figure 2.

VTVH MCD isotherms of D201GCl (orange, collected at 7,100 cm^{-1}) and D201G (light blue, collected at 11,100 cm^{-1}) Fe^{II}/αKG complexes and D201GCl (red, collected at 6,430 cm^{-1}) and D201G (blue, collected at 5,500 cm^{-1}) Fe^{II}/αKG/CAD complexes.

Author Manuscript Author Manuscript Author Manuscript Author Manuscript

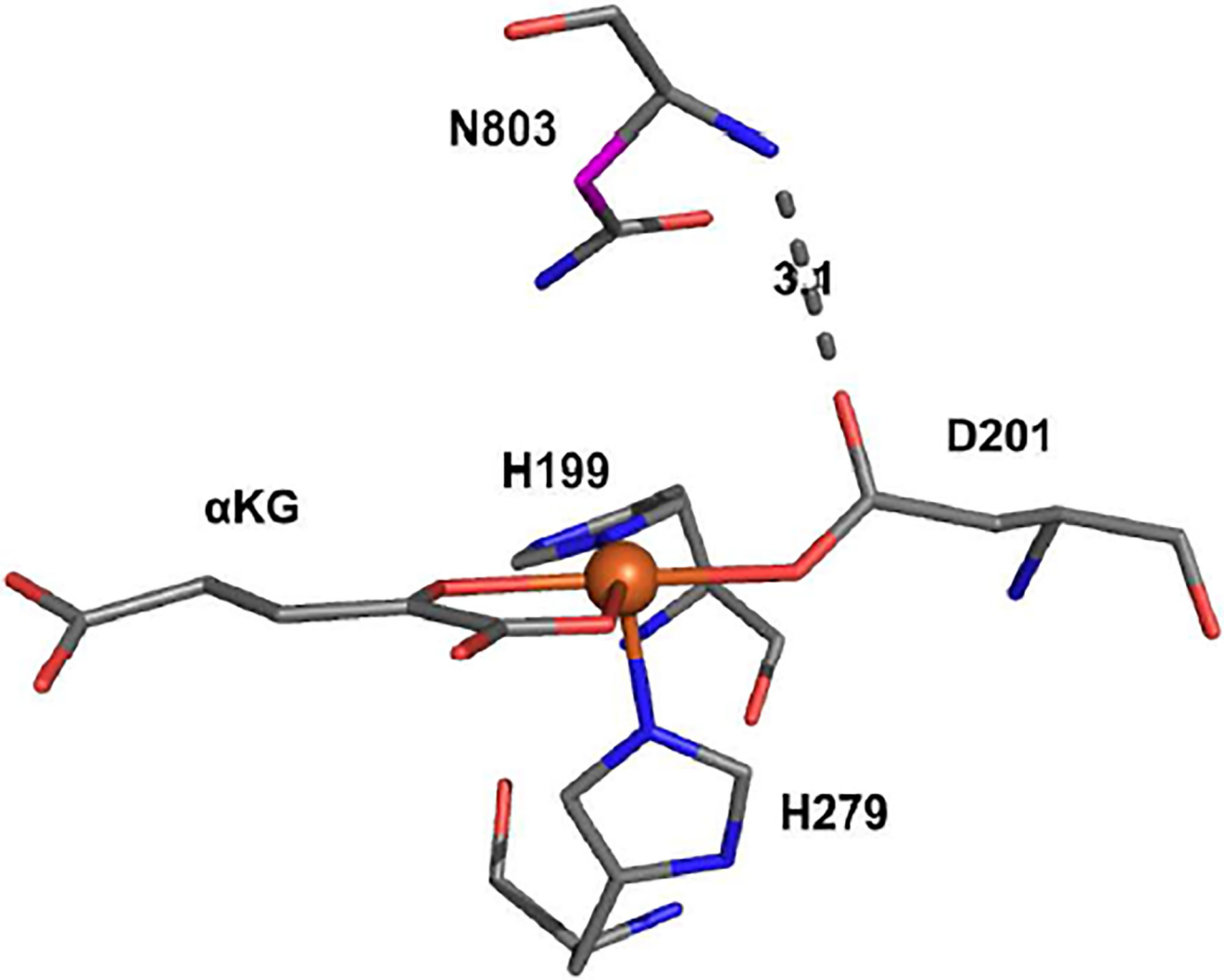

Figure 3.

Crystal structure of FIH ternary complex active site (1H2N) showing the H-bond between D201 and the N803 backbone amide. The carbon involved in HAA is highlighted in magneta.

Author Manuscript Author Manuscript Author Manuscript Author Manuscript

Table 1.

Gaussian resolved bands for the observed transitions reported in Figure 1 along with the values of their excited state splittings. All values are in cm^{-1}. [a]The second transition associated with this site is not observed and likely ~10,000 cm^{-1} from VTVH MCD spectroscopy. [b]Three transitions have been observed but the bands have not been assigned to a single Fe^{II} site.

Enzyme	Band 1	Band 2	Δ^5E
Fe^{II} Sites			
wt-FIH	8950	10700	1750
D201GCl	9200	11200	2000
D201G	9100	10950	1850
D201E	9050	10800	1750
D201A	9150	10950	1800
Fe^{II}/αKG Sites			
wt-FIH	8900	11100	2300
D201GCl	8950	11550	2600
	7400	[a]	
D201G	8900	11300	2400
D201E	8850	11550	2700
D201A	9100	11400	2300
Fe^{II}/αKG/CAD Sites			
wt-FIH	<5000	7950	>3000
	9000	11150	2150
D201GCl	<5000	9250	>4,250
	6200	10900	4,700
D201G	<5000	8800	>3800
	6100	11350	5,250
D201E[b]	8950	11500	>2,500
		14000	
D201A[b]	<5000	9100	>2,500
		11600	

Author Manuscript

Author Manuscript

Author Manuscript

Author Manuscript

Table 2.

Ground state parameters of the different αKG only and αKG+CAD bound complexes of the D201X variants. *All values in cm^{-1}. VTVH parameters for the *wt* enzyme are taken from ref. 19.

Variant	δ*	$g_{\|\|}$	Δ*	|V|*
Fe^{II} Sites				
wt-FIH	3.9	9.2	−275	100
Fe^{II}/αKG Sites				
wt-FIH	2.8	8.9	−950	530
D201GCl	2.5	9.05	−950 ± 100	475
D201G	5.0	8.0	950 ± 40	210
D201A	5.0	8.0	700 ± 80	330
D201E	2.4	8.9	−1100 ± 60	570
Fe^{II}/αKG/CAD Sites				
wt-FIH	1.8	9.2	−1200	410
D201GCl	3.7	8.0	1150 ± 50	480
D201G	4.0	8.0	1000 ± 80	340
D201A	5.3	8.0	700 ± 40	360

Author Manuscript

Author Manuscript

Author Manuscript

Author Manuscript

Table 3.

Initial rates of O_2 consumption and CAD hydroxylation for the different D201X variants. All values are in min^{-1} units. None of the other (Fe^{II}/αKG) variants consume O_2.

Variant	O_2 Consumption	CAD Hydroxylation
wt-FIH	16.3 ± 0.7	15.4 ± 0.6
D201GCl	1.9 ± 0.4	0.41 ± 0.03
D201G	0.3 ± 0.1	0.16 ± 0.01
D201E	1.7 ± 0.1	0.16 ± 0.02
D201A	<0.01	Not Detectable
D201E (No CAD)	1.67 ± 0.08	N/A